2012 2nd International Conference on Biomedical Engineering and Technology
IPCBEE vol. 34 (2012) © (2012) IACSIT Press, Singapore

Numerical Study of Stenosed Carotid Bifurcation Models Based on Wall Shear Stress Distribution

Kelvin K. L. Wong, Jingliang Dong and Jiyuan Tu

School of Aerospace, Mechanical and Manufacturing Engineering, RMIT University, PO Box 71 Bundoora VIC 3083, Australia

Abstract. We present the study of cardiovascular models based on medical image reconstruction and computational fluid dynamics, which can give rise to a virtual reality platform for flow analysis and a potential therapy planning tool for vascular diseases. Through comprehensive computational studies, the hemodynamic models of ten patient-specific carotid bifurcations are examined in terms of their geometries and flow properties. The characteristics of stenoses at various section of the anatomical structure are used as indicators for explaining the difference in flow properties such as wall shear stress. The case studies are based on different anatomies presented by the left, right or common carotid vessel, various degrees of geometrical non-planarity, and variation in severity of stenosis in carotid arteries for a group of patients. The success of this study presents the potential of using medical imaging and numerical simulation to provide existing clinical prerequisites for diagnosis and therapeutic treatment.

Keywords: Carotid bifurcation, numerical simulation, wall shear stress, stenosis.

1. Introduction

The application of medical image reconstruction for modeling vessel to use in CFD has been of rapid development in recent decades. Computational methods were first applied to generate velocity and pressure fields in idealized, generic models of vascular anatomy and physiology [1]. With the development of modern imaging technology, especially magnetic resonance imaging (MRI) and computed tomography (CT), it is now possible to quantify arterial blood flow in subject-specific physiologic models [2, 3]. For three-dimensional numerical studies, CFD models of the carotid artery can be constructed from MRA or CT images [4]. With the use of Computational Fluid Dynamic (CFD) simulations and MRI, the ability to evaluate complex relationship between hemodynamics and the prediction for atheroma may be possible [5]. For example, the artery can be studied and its wall shear stress is quantified using the governing Navier-Stokes flow equations.

The typical process for performing numerical simulation of blood vessel is based on medical imaging, image segmentation, 3D model reconstruction, grid generation and analysis. The final grid is used for numerical simulation of cardiac flow in the anatomy. Anatomical reconstruction of the arteries has facilitated the computational simulation of flow effectively. Human carotid bifurcation modeling can be performed more accurately, and the flow quantified based on CFD [6].

In terms of validating CFD results, phase contrast MRI velocimetry may be utilised. Such velocity-encoded MRI systems are able to extract the blood flow velocities in the cardiovascular anatomy in-vivo and may be visualised using color streamlines and vorticity contour plots. Based on MRI, we are able to perform image segmentation, geometry reconstruction and mesh generation. The physiological geometry can be imported into a CFD solver. In general, CFD simulation based on MRI plays an important role in evaluating the complex relationship between local hemodynamics and the prediction for atheroma. As such, this technique can be applied non-invasively at arterial sites where vascular anatomy typically exhibits substantial inter-individual variability.

2. Methods

2.1. Reconstruction of the Human Carotid Bifurcation

In our study, we performed imaging of six patients. Segmentation of the MRI was required to extract the geometry of the carotid vessels. The segmentation process includes thresholding and region growing [7], followed by 3D anatomical reconstruction [8] to obtain a very coarse solid model. During thresholding, a range of gray scale values are selected such that the region to be selected is of best contrast within this range. After the regions of interest were selected and extracted, the voxels are grouped together to form a 3D geometry. Then the reconstruction of carotid bifurcation anatomy into a Computer Aided Design (CAD) model is performed based on the segmentation information.

2.2. Details of Numerical Simulation

The fluid was assumed to have a density (ρ) of 1.176 g/cm^3 and viscosity (μ) of 4.0×10^{-3} Pa ·s and molar mass of 25 kg/kmol. Some of these values are referred from Ref [9]. The flow in our study is assumed to be Newtonian and the vessel walls are rigid. The time period T of one cardiac cycle is 0.92 s. The k-ω turbulence model was applied in the simulation. To ensure the convergence of each time step, the convergence criterion for the relative residual of all dependent variables was set to 1×10^{-4}. For time discretization, the second order backward Euler transient scheme was used.

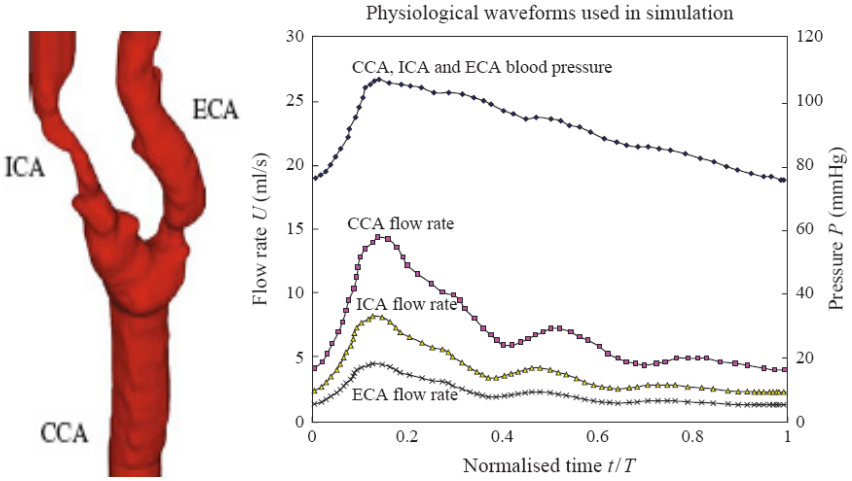

Fig. 1: Waveforms of flow rate and pressure of CCA, ICA and ECA.

A uniform pressure boundary condition varying with time was applied at the inlet cross-section of the CCA. For the inlet CCA pressure, values of 110 and 76 mmHg were used for the peak systolic and minimum of diastolic pressures respectively. For the downstream boundary conditions of the ICA and ECA, flow waveforms obtained from phase contrast MRI velocity measurements were used. A fully developed parabolic velocity profile was applied at the downstream end of both the ICA and ECA. The physiological waveform of the vessels' flow rates and blood pressure is shown in Fig. 1. The CAD geometry of the carotid bifurcation was imported into CFX-10.0 Solver using an Intel-P4. SSE2-WINT5.0 computer. To minimize the influence of initial flow conditions, all simulations were carried out for six cardiac cycles at T = 5.52 s. Based on a sample subject, we found that the total number of nodes (numbering 100,278) with total number of elements/tetrahedrons (at 500,830) is sufficient in the case. Comparing its predicted maximum velocity at the stenosed region with that of the fine mesh simulation, only 0.2% discrepancies were observed.

2.3. Details of Case Studies

A total of ten carotid bifurcation models (with different branching and degrees of stenosis) were selected for the simulation. The case study subjects are labelled as (1) to (6) with the denotation (/L) and (/R) representing the left and right carotid bifurcations respectively. The flow properties of the (/L) and (/R) bifurcations will be compared. Then the flows of different patients at the same location of their blood vessels are to be compared to analyze the relationship between the geometry and blood flow property. The flow parameters to be discussed include geometry, pressure gradient and wall shear stress.

3. Results

3.1. Comparison of Anatomical Geometries

Individual variation in the anatomy of arteries in human may be considerable. All the bifurcations exhibit some degree of geometrical non-planarity, subject (1/L) and (3) being more planar, while (1/R), (2/L) and (2/R) are highly non-planar. The degree of blockage is defined by using percent reduction in area. The ECA for subject (1/L) is approximately 60% blocked, whereas ICA that pertains to subject (1/R) shows more severe blockage (up to 70% of the vessel was blocked). Blood vessel on (2/L) and (2/R) are slightly stenosed (Approximately 40% blockage).

We present the comparison for ICA and ECA stenoses based on the ten case studies from the six patients (Tab. 1). Patients (1/L), (1/R), (5/R) and (6) have severe stenoses at the ICA, with ICA to CCA ratios of 9%, 10%, 23% and 25% respectively, and patients (4/L) and (5/R) are heavily stenosed at the ECA with ratios of 23% and 12% respectively. Although not displayed in the table, it may be worth noting that the CCA that pertains to patient (4/L) has an area that is reduced to 5.0 mm^2 at its bifurcation. Also, the CCA area for patient (5/R) is observed to reduce till 14 mm^2 at bifurcation.

Tab. 1: Comparison of stenosis for ICA and ECA with respect to CCA.

Comparison of carotid bifurcation stenosis										
Patients	**(1/L)**	**(1/R)**	**(2/L)**	**(2/R)**	**(3)**	**(4/L)**	**(4/R)**	**(5/L)**	**(5/R)**	**(6)**
CCA (mm^2)	32.1	30.3	20.2	24.5	28.7	41.0	24.1	27.3	31.6	34.6
ICA (mm^2)	2.9	3.0	9.8	12.1	12.7	13.5	8.0	8.7	7.2	8.8
ICA to CCA ratio (%)	9	10	49	49	44	33	33	32	23	25
ECA (mm^2)	17.8	11.7	4.7	6.8	11.2	9.3	8.0	7.1	3.8	14.0
ECA to CCA ratio (%)	55	39	23	28	39	23	33	26	12	40

The geometry of subject (3) was taken from a healthy person whose carotid bifurcation shows no signs of stenosis. The CCA, ICA and ECA diameters of our measured sample are 6.00 mm, 3.98 mm and 3.96 mm respectively, while the diameters of the standard anatomy are 6.2 mm (at CCA), 4.4 mm (at ICA) and 3.5 mm (at ECA). The angle between the ICA and ECA is approximately 40˚, which is a small deviation as compared with the standard geometry at 50˚.

3.2. Comparison of Wall Shear Stress

It has been indicated by previous studies that wall shear stress promotes luminal thinning and plaque rupture [10-12] and low WSS regions are more prone to athersclerosis [13]. The growth of lesion will lead to stenosis at the artery wall, and further narrowing downstream of the blood vessel will occur. Therefore, this is one of the key parameters that we will use for examination of diseased carotid bifurcations.

Topological maps of the predicted maximum wall shear stress at peak pressure for each of the ten case studies are given in Fig. 2. In all of the models, the maximum wall shear stress (WSS_{max}) is shown to have peak values on the inner walls of ICA and ECA near the bifurcation points, and significantly elevated values spiralling around the larger angular branch (either the ICA or ECA) from the inner walls along the superior orientation. The maximum WSS value appeared at the stenosed section due to vessel tapering. For example, locations where stenosed areas of the ICA branch on cases (1/L), (1/R), (4/R), (2/L) are shown to have maximum wall shear stress.

Low wall shear stress was seen primarily at the roots and along the outer walls of the sinus bulbs. Nevertheless, the shape and location of the wall surface subject to low wall shear stress differ from subject to subject. For all cases, the low WSS zone starts from the CCA and extends asymmetrically to the posterior and anterior aspects, with more pronounced coverage on the ECA walls in subjects (1/L), (1/R), (2/L), (2/R), (4/R) and (3). On the contrary, this pattern is reversed in cases (5/L), (5/R) and (6). For subject (4/L), the low WSS zone starts from CCA, and then terminates at the stenosed area, which is located at the CCA just before the bifurcation, and then appears again on the outer wall of ICA branch. The ranking of WSS_{max} is presented by Tab. 2 for ten cases.

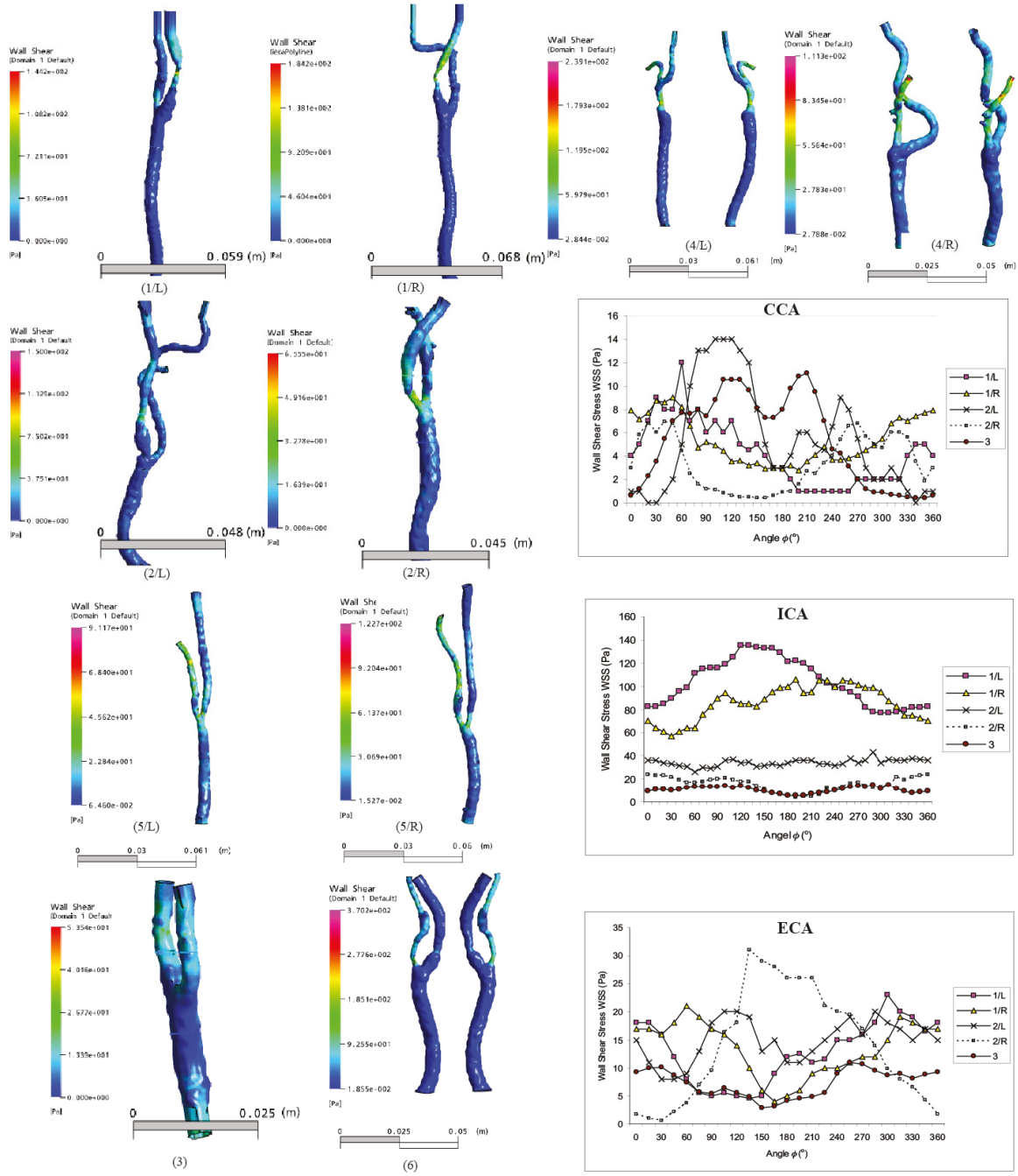

Fig. 2: Wall shear stress surface plot of carotid bifurcations and comparison at CCA, ICA and ECA sections..

Tab. 2: Maximum wall shear stress comparison among ten case studies.

Locations and values of maximum WSS		
Patients	**Locations**	***WSS*$_{max}$ (Pa)**
(6)	ECA branch	370
(4/L)	CCA near bifurcation	239
(1/R)	ICA branch	184
(2/L)	ICA branch	150
(1/L)	ICA branch	144
(5/R)	Bifurcation and ECA branch	123
(4/R)	ICA branch	113
(5/L)	Bifurcation and ECA branch	91
(2/R)	ICA branch	65.5
(3)	ICA branch	53.5

Planes are used for analysis on the CCA, ICA and ECA of five selected subjects. Wall shear stresses along the planes are calculated and are compared with each other (Fig. 2). The ECA and ICA sections are selected at the stenosed location (at place of smallest diameters), whereas the CCA sections were selected at a common location that is typically located at approximately three times the CCA diameter below its bifurcation. The wall shear stress is chosen at the time of peak systole.

No common trend exists for the patients. Based on the CCA planes of the five subjects, values of WSS for (1/L), (2/L) and (3) vary more than those for (1/R) and (2/R). For example, the maximum WSS for patient (1/L) is 14 Pa and its minimum value is 0 Pa, which results in a difference of 14 Pa. But WSS that pertains to case subject (1/R), which ranges from 2.8 to 9 Pa, has a difference of 6.2 Pa. This may be the result of large geometry change in cross sectional area for patient (1/L).

4. Conclusion

Carotid bifurcations of six case subjects at different locations constitute a total of ten cases for our study. We examined different geometry and conditions of the vessel, such as the left or right carotid, severely or slightly stenosed carotid arteries. In particular, we simulate the hemodynamics at bifurcation for analysis and discussion. Flow patterns are shown to be highly dependent on the anatomical geometry. Based on our analytical evaluation and comparison, we have built a relationship between flow properties and geometry variations qualitatively and quantitatively. We have compared the flow property for the left and right carotid vessels of every patient, and evaluate the flow for different patients at the same location to establish the relationship between the stroke and hemodynamics.

5. Acknowledgments

The financial support provided by the Australian Research Council (ARC project ID DP0986183) is gratefully acknowledged.

6. References

[1] Taylor, C.A. and M.T. Draney, *Experimental and computational methods in cardiovascular fluid mechanics.* Annual Review of Fluid Mechanics, 2004. **36**: p. 197-231.

[2] Phillips, *Philips Medical Systems Clinical Education, Basic principles of MR imaging,*, 1984.

[3] Powell, A.J., et al., *Phase-Velocity Cine Magnetic Resonance Imaging Measurement of Pulsatile Blood Flow in Children and Young Adults: In Vitro and In Vivo Validation.* Pediatric Cardiology, 2000. **21**: p. 104-110.

[4] Merrifield, R., et al., *Combined CFD/MRI Analysis of Left Ventricular Flow*, in *Proceedings of the Medical Image and Augmented Reality 2004*2004. p. 229-236.

[5] Marshall, I., et al., *MRI and CFD studies of pulsatile flow in healthy and stenosed carotid bifurcation models.* Journal of Biomechanics, 2004. **37**(5): p. 679-687.

[6] Long, Q., et al., *Quantitative comparison of CFD predicted and MRI measured velocity fields in a carotid bifurcation phantom.* Biorheology, 2002. **39**(3-4): p. 467-474.

[7] Gonzalez, R.C. and R.E. Woods, *Digital Image Processing, 2nd edition*2002: Prentice-Hall, Inc., New Jersey, USA.

[8] Chandran, K.B., et al., *Coronary Arteries: Imaging, Reconstruction, and Fluid Dynamic Analysis.* Critical Reviews in Biomedical Engineering, 2006. **34**(1): p. 23-103.

[9] Khan, I., J. Oshinski, and C. Aidun, *Correlation between shear stress and wall thickening in human carotid artery: I. preliminary repeatability studies of MRI data.* Proceedings of the 5th IASTED International Conference: biomedical engineering, 2007: p. 209-214.

[10] Berger, S.A. and L.D. Jou, *Flows in stenotic vessels.* Annual Review of Fluid Mechanics, 2000. **32**: p. 347-382.

[11] Gertz, S.D., et al., *Endothelial cell damage and thrombus formation after partial arterial constriction: relevance to the role of coronary artery spasm in the pathogenesis of myocardial infarction.* Circulation, 1981. **63**: p. 476-486.

[12] Zohdi, T.I., *A simple model for shear stress mediated lumen reduction in blood vessels.* Biomechanics and Modeling in Mechanobiology, 2005. **4(1)**: p. 57-61.

[13] Plank, M.J., et al., *Modelling the Early Stages of Atherosclerosis*, in *Mathematical Modeling of Biological Systems, Volume I*2007, Birkh\"auser Boston. p. 263-274.